Nanoscale

RSC Publishing

REVIEW

View Article Online
View Journal | View Issue

Visible light driven type II heterostructures and their enhanced photocatalysis properties: a review

Cite this: *Nanoscale*, 2013, **5**, 8326

Yajun Wang, Qisheng Wang, Xueying Zhan, Fengmei Wang, Muhammad Safdar and Jun He*

Considerable efforts have been devoted to enhancing the photocatalytic activity and solar energy utilization of photocatalysts. The fabrication of type II heterostructures plays an important role in photocatalysts modification and has been extensively studied. In this review, we briefly trace the application of type II heterostructured semiconductors in the area of environmental remediation and water splitting, summarize major fabrication methods, describe some of the progress and resulting achievements, and discuss the future prospects. The scope of this review covers a variety of type II heterostructures, focusing particularly on TiO_2 and ZnO based visible light driven type II 0D and 1D heterostructured photocatalysts. Some other low dimensional nanomaterials which have shown high-performance photocatalysis are also presented. We expect this review to provide a guideline for readers to gain a clear picture of fabrication and application of type II heterostructures.

Received 30th March 2013
Accepted 19th May 2013

DOI: 10.1039/c3nr01577g

www.rsc.org/nanoscale

1 Introduction

Environmental and energy issues are among the biggest challenges in the new century. With the growth of worldwide industry, severe environmental contaminations have become a major concern of our society. The development of high efficiency, green energy sources and eco-friendly methods for environmental remediation has become an imperative task. Moreover, energy shortages and surging green-house gas (GHG) emissions have been two of the major challenges the world is facing today. For example, in China over 70% of domestic energy originates from coal. As a result, China suffers from a series of environmental problems and public health crises due to the burning of fossil fuel. In order to solve these severe problems, China has set goals to mitigate its CO_2 emission per unit of Gross Domestic Production (GDP) by 40–45% by 2020, with an interim target in the 12th 5-Year Plan of 17% by 2015.[1]

Among various strategies, finding renewable energy, instead of fossil fuel is the key measure. Hydrogen, as a clean and non-carbon energy source, is of great potential in solving the environmental crisis and energy shortage. As a result, photocatalysis, as one of the promising technologies in utilizing solar energy to solve environmental and energy issues, has attracted considerable attention.

Fujishima and Honda first reported the UV light induced photo-assisted decomposition of water into hydrogen and oxygen using a titanium dioxide photoanode in electrochemical

National Center for Nanoscience and Technology, Beijing 100190, P. R. China. E-mail: hej@nanoctr.cn

Yajun Wang received her BS degree in Environmental Engineering from Tsinghua University in 2006. She received her PhD degree in Chemistry from Tsinghua University in 2011. Currently, she is an assistant professor in National Center of Nanoscience and Technology (NCNST), China. Her research interests include development and modification of photocatalysts for environmental purification and water splitting.

Jun He received his PhD in physical chemistry from the Institute of Semiconductors, Chinese Academy of Sciences in 2003. Dr He is presently a Professor of physical chemistry of materials in the National Center for Nanoscience and Technology, China, with research interests in low dimensional semiconductor materials synthesis, characterization, and devices.

cell in 1972.[2] Since then, semiconductor photocatalysis has attracted widespread attention in scientific community due to its potential application in environmental remediation and hydrogen production. The basic mechanisms of photocatalysis have been established and reported in many literature accounts.[3,4] Taking TiO_2 as an example, the mechanism of the photocatalytic process is shown in Fig. 1.

When the absorbed photon has an energy equaling or exceeding the band gap energy (E_g) of TiO_2, an electron in the filled valence band (VB) is excited into the empty conduction band (CB), leaving behind a hole in VB (stage I). Stage II and stage III occur in parallel, but the recombination process (stage II) is much faster than the transportation process (stage III) as shown in Fig. 1. After the electrons and holes transfer to the active sites of the surface of TiO_2, they will act as reducing/oxidizing agents to drive reduction/oxidation on the surface (stage VI and V). In detail, at stage VI and V, for photocatalytic degradation of pollutants, holes of VB can react with surface adsorbed H_2O to produce hydroxyl radicals. The hydroxyl radicals are strong oxidizing agents, which can oxidize almost all organic pollutants with no selectivity. Moreover, the holes can also directly oxidize the organic pollutants to form R^+.[3,5] For water splitting, water molecules are reduced by the photoinduced electrons to form H_2 and are oxidized by the photoinduced holes to form O_2. For effective water splitting, the bottom level of the CB of the semiconductor has to be more negative than the redox potential of H^+/H_2 (0 V *vs.* NHE), while the top level of the VB of the semiconductor should be more positive than the redox potential of O_2/H_2O (1.23 V *vs.* NHE). The minimum band gap for water splitting is 1.23 eV; theoretically, all types of semiconductors that satisfy the above requirements could be used as photocatalysts for water splitting. Particularly, in a photoelectrochemical (PEC) cell, carriers in the semiconductor should travel to an electrode/liquid junction to drive the hydrogen/oxygen evolution reaction. In electron-transfer processes at semiconductor/liquid junctions, unavoidable losses are caused by concentration and kinetic overpotentials. Therefore, accounting for the losses, the energy required for PEC water splitting at a semiconductor photoelectrode is calculated as 1.6–2.4 eV per electron–hole pair generated.[6]

Although semiconductor photocatalysis has made great progress during the past three decades, there are still some unsolved problems. Again, taking TiO_2 as an example, TiO_2 is known as the most widely investigated photocatalyst due to its high oxidative efficiency, high chemical stability, nontoxicity and low-cost.[7–9] Presently, the photocatalytic degradation activity and water splitting efficiency of TiO_2 is still low, mainly due to the following two reasons: (1) slow reaction rate: the photocatalytic reactions only occur when the photoinduced electrons and holes transfer to the surface active sites of the semiconductor. However, the recombination process is much faster than the transportation process, leading to low photocatalytic efficiency. (2) Poor solar energy utilization: TiO_2 with a bandgap of 3.2 eV can be only excited by photons with light wavelengths shorter than about 400 nm in the UV wavelength range, which accounts for about 4% of the solar radiation energy.[10,11] Therefore, a great deal of effort has been devoted to enhancing the efficiency of the photocatalytic process and extending the light adsorption range of TiO_2, such as formation of semiconductor heterostructures,[12,13] codeposition of noble metals,[14,15] doping,[16,17] surface hybridization[18–20] and coupling with other technology.[19,20] Among these approaches, formation of semiconductor heterostructures is an effective way to enhance the photoinduced charges separation efficiency and the photocatalytic performance, and has been extensively studied for the last decades. Depending on the bandgaps and the electronic affinity of semiconductors, semiconductor heterostructures can be divided into three different cases: type-I, type-II and type-III band alignment as shown in Fig. 2.

In a type-II band alignment, the position of valance and conduction bands of semiconductor 2 is higher than that of semiconductor 1, and the steps in the conduction and valance bands go in the same direction. Importantly, the difference of chemical potential between semiconductor 1 and 2 causes band bending at the interface of junction. The band bending induces a built-in field, which drives the photogenerated electrons and holes to move in opposite directions, leading to a spatial separation of the electrons and holes on different sides of heterojunction.[21] Thus, the formation of type-II heterostructures is an effective approach to enhance charge separation efficiency for improved photocatalytic degradation activity and water splitting efficiency.

Moreover, a UV excited semiconductor (such as TiO_2, ZnO, $ZnWO_4$) coupled with a visible light excited semiconductor

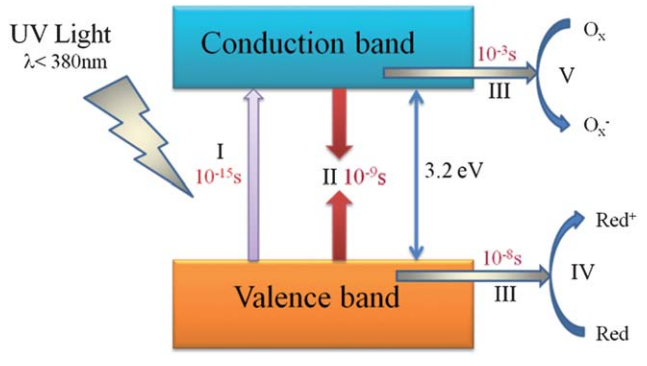

Fig. 1 Primary steps in the photocatalytic mechanism (TiO_2): (I) formation of electron (e^-)–hole (h^+) pairs by photoexcitation; (II) photoinduced charge recombination; (III) photoinduced charge transportation; (IV) oxidation caused by a valence band hole; (V) reduction caused by a conduction band electron (adapted with permission from ref. 3, copyright 1995 American Chemical Society).

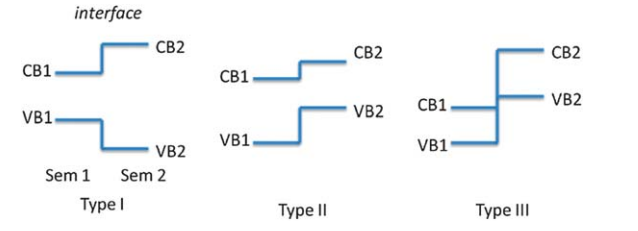

Fig. 2 Schematic energy band diagram of three types of semiconductor heterojunctions.

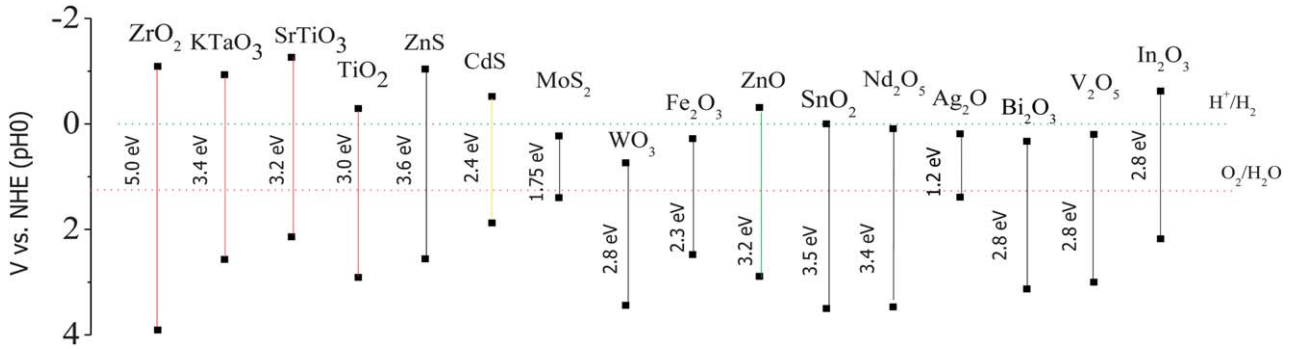

Fig. 3 Band edge position of several semiconductors, using the normal hydrogen electrode (NHE) as a reference (adapted with permission from ref. 23, copyright 2009 Royal Society of Chemistry).

(a narrow bandgap semiconductor such as CdS, CdSe, CdSSe, C_3N_4) can effectively improve its solar energy utilization efficiency because the synergic absorption of two semiconductors with different band gaps extends the light response range to the whole solar spectrum. There are two prerequisite conditions to prepare a visible light driven type II heterostructure: (1) the outer shell material should have a strong visible light absorption (photo-sensitizer), and (2) the band alignment at the interface between the outer shell material and inner core should satisfy the conditions of type II heterostructures. In addition, the crystal structure in the junction area of the heterostructure is found to be important in enhancing the quantum efficiency of the photocatalyst. A difference in lattice spacing between two semiconductors is likely cause lattice mismatch. The lattice mismatch at the interface may cause defects, which trap the photogenerated carriers and thus prevent the diffusion of electrons and holes. However, interface strain arising from the lattice mismatch also alters the electronic structure. Indeed, lattice strain could induce an electric field, which further improves the separation efficiency of electrons and holes.[22] Consequently, careful selection of materials should be taken before preparing visible light driven type II heterostructures. Fig. 3 shows the band edge position of several widely used semiconductors.[23] The type-II heterostructure has attracted widespread attention in fabrication, study of its properties, and applications. Diverse type-II heterostructures have been explored, such as composite nanoparticles,[24–29] quantum dots in nanowires,[30–32]core/shell nanowires,[33–35] *etc.* Compared with pure semiconductors, these type-II heterostructures, such as CdS/TiO_2,[36,37] CdS/ZnO,[38,39] ZnSe/ZnO,[40] ZnS/ZnO,[41] $ZnO/TiO_2/CuO$,[42] and SnO_2/CdS[43] have achieved higher photocatalytic efficiency and solar energy utilization. In this review, we briefly trace the application of type II heterostructured semiconductors in the area of environmental remediation and water splitting, summarize major fabrication methods, describe some of the progress and resulting achievements, and discuss the future prospects.

2 Synthesis of type II heterostructures

Due to their wide application in the degradation of pollutants, energy conversion and water splitting, controllable synthesis of visible-light driven type II heterostructured photocatalysts have attracted tremendous attention. Over the past decades, various synthesis techniques, such as chemical vapor deposition,[44] chemical deposition,[45–47] electrodeposition, *etc.*,[48] have been well developed and successfully used in preparing high-quality type II core/shell heterostructures.

Compared with the synthesis of the core material, the growth of outer shell material (sensitizer) is more complicated. For example, different thicknesses of sensitizer may result in different photocatalytic properties.[49] Therefore, in this section, we will focus our attention on methods for the synthesis of the sensitizer. Considering the wide application of ZnO and TiO_2 as the photocatalysts, here we will mainly discuss the preparation of sensitizers based on ZnO and TiO_2 nanostructured material. Other type II heterostructured photocatalysts prepared by special synthetic methods are also presented.

2.1 Chemical vapor deposition

Vapor-phase synthesis is probably the most extensively explored approach in the field of nanofabrication. Chemical vapor deposition (CVD) or chemical vapor transport (CVT) is very commonly used for type II heterostructure synthesis. This method has the ability to control the sensitizer composition, thickness and stability by controlling several processing parameters such as temperature, pressure, carrier gas, substrate and evaporation time period. A number of type-II heterostructured sensitizers, for example, CdSe, CdSSe, $Zn_xCd_{1-x}Se$, ZnS_xSe_{1-x}, ZnS_xSe_{1-x}/ZnSe, $ZnGa_2O_4$ and ZnTe have been deposited on ZnO cores *via* the CVD method.[44,50–54] In most cases, type II heterostructure can be obtained in two-step growth procedure. Firstly, the inner core semiconductor nanostructure is grown on a suitable substrate *via* CVD or another synthetic technique. In the second step, the substrate with pre-grown core nanostructure, is kept in a tube furnace to deposit the shell and under optimized conditions, controlled shell materials can be obtained. Myung and co-workers have reported 10 nm and 50 nm thick CdS shells on ZnO nanowires which were remarkably associated with time and temperature variation.[50]

Our group has recently successfully synthesized a ZnS_xSe_{1-x} shell on a vertical ZnO nanowire array *via* the CVD method.[44]

Firstly, a single crystalline ZnO nanowire array was obtained on an Au deposited Si substrate using a two-zone furnace tube and mixed graphite and ZnO powder as sources. In the second step, a homogenous shell of ZnS_xSe_{1-x} was deposited on the exposed surface of ZnO by CVD. In detail, ZnS and ZnSe mixed in a 3 : 7 mole ratio were used as the source in the center of a quartz tube keeping 8 cm of distance from the pre-grown ZnO nanowire substrate. The source was evaporated at 1100 °C and deposited on the ZnO nanowire array, and the shell thickness was carefully controlled by adhering to the optimum deposition time. The synthesized core/shell structure is presented in Fig. 4. Fig. 4a represents the ZnO nanowire before coating (inset of Fig. 4a) and after ZnSSe coating. X-ray EDS spectra demonstrate that the core and shell have an approximate 1 : 3 atomic ratio (Fig. 4b). Transmission electron microscopy (TEM) investigation confirms that the synthesized material was a typical core/shell structure and with a fine single crystalline structure as shown in Fig. 4c and d.

2.2 Chemical deposition

Chemical deposition is a simple and low cost method to fabricate type-II heterostructures. In this technique, the growth of thin films results from the bulk precipitation of the solution.[55] Chalcogenide layers are usually prepared by this method. The temperature, pH, deposition time, and the concentration of the precursor play important roles in this method. Based on this method, some type II heterostructures can be easily obtained,[56,57] such as CdS/TiO_2,[45] CdSe/CdS/ZnO,[46] $Zn_xCd_{1-x}S/ZnO$,[47] CdS/ZnS,[58] g-C_3N_4/TiO_2.[59]

For example, TiO_2/CdS heterostructure can be obtained by a chemical bath deposition method.[45] Firstly, the TiO_2 core was prepared by a hydrothermal method, and then further converted into an ITO substrate, which was vertically immersed in an aqueous bath containing 10 mL 0.02 M $CdCl_2 \cdot 2.5H_2O$, 10 mL 0.2 M CH_4N_2S, 10 mL of 1.5 M $NH_4NO_3$and 10 mL 0.5 M KOH to deposit the CdS shell at 85 °C. Typical SEM and TEM images of the TiO_2/CdS are shown in the Fig. 5. This facile method was also used in another example to fabricate heterostructured $Zn_xCd_{1-x}S/ZnO$.[47] The morphologies of the $ZnO/Zn_xCd_{1-x}S$ heterostructure could be controlled by altering the ratio of the $Zn_xCd_{1-x}S$ precursors.

2.3 Electrochemical deposition

Compared with the CVD method, electrochemical deposition allows large-scale nanostructure fabrication at low temperature. This conventional technique is most suitable for production of highly dense, uniform and ordered type-II heterostructured nanomaterials for large scale applications.[60–64] The shell thickness of type-II heterostructures, which directly influences their performance, can be controlled by temperature, potential and time duration. For instance, Yao and co-workers reported that the thickness of CdS shell on ZnO nanorod can be controlled by this method *via* adjustment of deposition time.[60] In addition, Wu and co-workers synthesized Co_3O_4 nanowires on Ni foil by a hydrothermal method and then used this material as the working electrode for electrodeposition of an NiO shell. Co_3O_4 nanowires can be covered by the NiO nanoflake shell when 0.25 mA cm^{-2} constant anodic current was applied for 1 h.[64]

In the electrodeposition system, the pre-grown materials on indium-doped tin oxide (ITO), fluorine-doped tin oxide (FTO) or other relevant substrates is used as the working electrode. As a representative case, the large scale electrodeposition of a CdTe shell on a ZnO nanorod array was reported by Wang and co-workers.[48] A thermally evaporated ZnO nanorod array on ITO was used as the working electrode, Pt foil as the counter electrode and saturated calomel electrode (SCE) as the reference

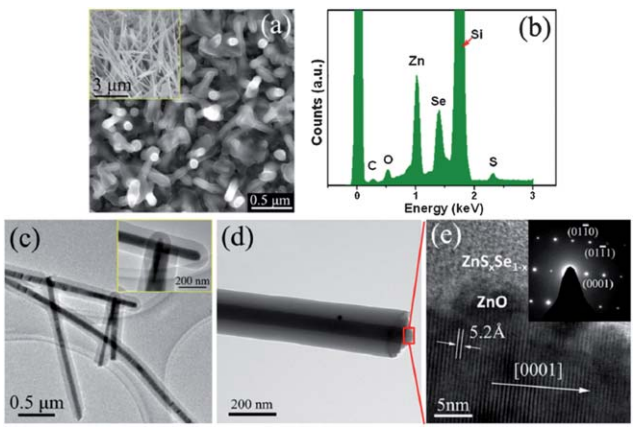

Fig. 4 (a) SEM image of ZnS_xSe_{1-x}/ZnO core/shell nanowires, inset is a side-view SEM image of ZnO nanowires before coating, (b) an X-ray EDS of ZnS_xSe_{1-x}/ZnO core/shell nanowires. (c) and (d) TEM images of ZnS_xSe_{1-x}/ZnO core/shell nanowires along inset of enlarged head ends. (e) HRTEM images of a single ZnS_xSe_{1-x}/ZnO core/shell nanowire, inset SAED pattern of the core/shell nanowire (reprinted with permission from ref. 44, copyright 2012 American Institute of Physics).

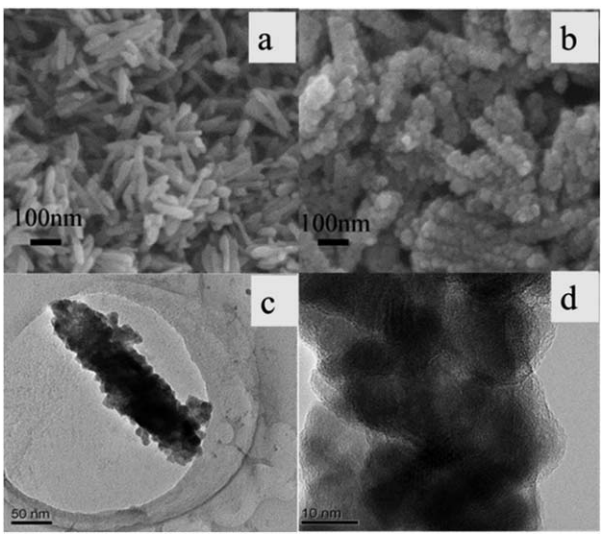

Fig. 5 SEM images of the as-prepared TiO_2 nanorod film before (a) and after (b) coating with CdS nanoparticles at high magnification; TEM image of a single CdS/TiO_2 core/shell nanorod (c) and high-resolution TEM image of a single CdS/TiO_2 core/shell nanorod (d) (reprinted with permission from ref. 45, copyright 2007 Elsevier).

electrode. Electrodeposition of the CdTe shell was completed by applying −1.0 V *versus* SCE in TeO_3^{2-} and Cd^{2+} electrolyte solution with pH 8.3. The thickness of the CdTe shell was controlled by maintaining the total charge of the electrodeposition system. Fig. 6a and c display SEM images of the bare ZnO nanorod array. Fig. 6b and d show the SEM images of ZnO nanorods after CdTe electrodeposition. The TEM image in Fig. 6e reveals the smooth covering of the ZnO core with an 11 nm CdTe shell, and the HRTEM image in Fig. 6f depicts the crystalline structure of CdTe/ZnO nanocable. As demonstrated by these examples, electrochemical deposition is a suitable technique to fabricate controlled type-II heterostructures.

2.4 Ion exchange

Ion exchange is a novel technique to prepare core/shell heterostructures by exchanging the ions at the interface of the heterostructure. In this method, the anion or cation is transferred into the nanostructure, then the shell is formed in gas or solution phase. In the process of cation exchange,[65] external cations enter the parent crystal at the same time as the original cations diffuse out of the crystal. For example, Konenkamp and Dloczik have proved that the oxygen component of highly structured ZnO films can be replaced by S in the H_2S phase and thus a ZnS shell with similar morphology to the initial ZnO was obtained.[66] Meanwhile, through the exchange of metal ions in solution, synthesis of columnar and tubular films of Ag_2S, Cu_2S, Bi_2S_3, or Sb_2S_3 has been achieved from columnar ZnO.[66] Khanchandani and the co-workers[67] have synthesized CdS/ZnO core/shell nanorod arrays through an ion exchange reaction between $[Zn^{2+}O^{2-}]$ ions and $[Cd^{2+}S^{2-}]$ ions. The thickness of the shell can be controlled by adjusting the amounts of precursors. The different morphologies of ZnO nanorods and CdS/ZnO are shown in the Fig. 7. The comparison of photocatalytic properties, photoluminescence (PL), and absorbance band of ZnO nanorods and CdS/ZnO is shown in Table 1.

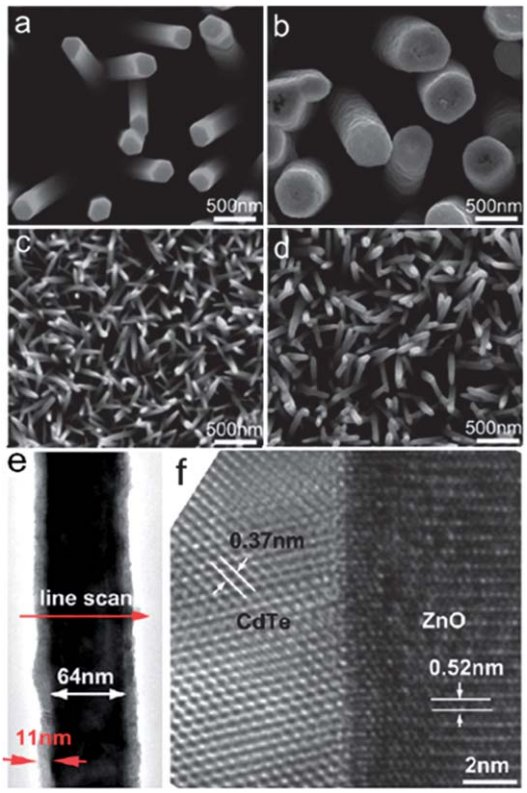

Fig. 6 ZnO nanorod arrays (a) before and (b) after electrodeposition (160 nm thick shell) with total charge of 6.7 C; ZnO nanorod arrays (c) before and (d) after electrodeposition (11 nm thick shell) with total charge of 0.7 C. (e) Low-magnification TEM image showing the uniform morphology of a single CdTe/ZnO nanocable; (f) typical HRTEM image taken from the same CdTe/ZnO nanocable, showing the interface and crystalline structure of the nanocable (reprinted with permission from ref. 48, copyright 2010 American Chemical Society).

2.5 Successive ionic layer adsorption and reaction

The "successive ionic layer adsorption and reaction" (SILAR) technique is another facile synthetic method to fabricate type-II core/shell heterostructures. This method was proposed by Nicolau[68] in 1985. It is a heterogeneous chemical reaction at the solution–solid interface on which the cations and anions are absorbed. This reaction is as follows: $m[CLp]^{n+} + n[AL'q]^{m-} \rightarrow C_mA_n\downarrow + mpL + nqL'$. Here, L and L′ stand for different ligands and $[CLp]^{n+}$and $[AL'q]^{m-}$ are cations and anions. After each immersion, the substrate with core/shell arrays should be rinsed by deionized water. The shell synthesized by SILAR can achieve better photoluminescence properties than those of shells synthesized by other methods.

For example, Lee and Yong[49] fabricated CuS nanoparticle/ZnO nanowire heterostructures on a mesh substrate. In this process, uniform CuS NPs were deposited on the pre-grown ZnO NWs array through SILAR. The synthesized CuS/ZnO heterostructured NWs exhibited superior photocatalytic activity under visible light illumination compared with that of the pure ZnO NWs. In addition, type-II heterostructured PbS/CdS p–n junctions have also been synthesized by successive cation exchange.[69] Moreover, the photoelectrochemical activity of this structure could be tuned by changing the size and density of the PbS nanoparticles on the CdS nanowires. The morphology of this nanostructure is shown in Fig. 8.

2.6 Solvothermal/hydrothermal method

The methods mentioned above are normally utilized to synthesize core/shell structures on substrates. For the preparation of powdery type II heterostructured photocatalysts, these

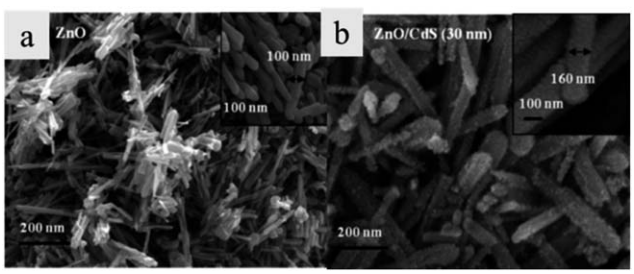

Fig. 7 FESEM images of (a) ZnO nanorods and (b) CdS/ZnO nanorods (reprinted with permission from ref. 67, copyright 2012 American Chemical Society).

Table 1 Absorbance band, PL band, current, and photocatalytic efficiency of ZnO and CdS/ZnO core/shell nanorod arrays with varying shell thickness (reprinted with permission from ref. 57, copyright 2012 American Chemical Society)

Sample	Shell thickness (nm)	Absorbance band (nm)	PL band (nm)	Current (A)	Photocatalytic efficiency (%)
ZnO		372	380	9.22×10^{-7}	70.0
ZnO/CdS1	10	425	460	8.09×10^{-6}	85.0
ZnO/CdS2	15	442	473	1.62×10^{-5}	91.5
ZnO/CdS3	30	465	490	1.75×10^{-5}	98.0

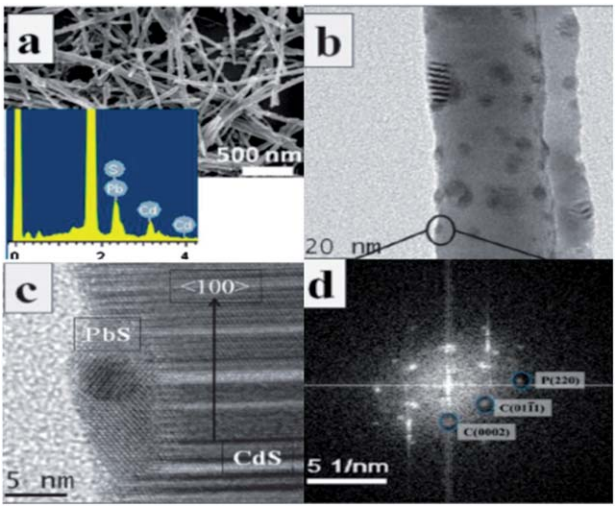

Fig. 8 (a) SEM image of PbS/CdS synthesized by a cation exchange method, inset is EDX of the heterostructure. (b) TEM image showing a section of the nanowire with islands. (c) HRTEM indicating the presence of CdS and (d) FFT (SAED) pattern confirming the formation of PbS (reprinted with permission from ref. 69, copyright 2012 Royal Society of Chemistry).

methods are not the ideal choices due to the fact that powdery heterostructures are always dispersed in the solution. Solvothermal/hydrothermal methods, where the reaction occurs in a solvent, are one of the most commonly used preparation methods of powdery nanostructures.[24,70–73] In a typical process, the mixture of a reagent such as amines and a precursor with appropriate ratio are injected in to a solvent which not only accelerates the dissolution of precursor but also speeds up the reaction rate between precursor and reagent with the increase of pressure and temperature. A pronounced advantage of this method is that most materials can be dissolved in appropriate solvent by modulating the temperature and pressure. In the case of the synthesis of $AgIn_5S_8/TiO_2$ heterojunction nanocomposites,[72] the mixture of TiO_2, thioacetamide, $AgNO_3$ and $In(NO_3)_3 \cdot 4.5H_2O$ were dissolved in distilled water. After adjusting the pH value of the mixed solution to 10.2, it was then sealed in a Teflon-lined autoclave. Keeping the temperature at 180 °C for 24 h, the $AgIn_5S_8/TiO_2$ heterojunction nanocomposite was precipitated. Interestingly, Yu and co-workers developed a microemulsion-mediated solvothermal synthetic method that simplifies the formation of CdS/TiO_2 nanocomposites.[24] In detail, titanium isopropoxide was first added into Millipore water (microemulsion A), and then $Cd(NO_3)_2$ (microemulsion B) and $(NH_4)_2S$ (microemulsion C) were successively added in the mix solution. With simultaneous coprecipitation of $Cd(NO_3)_2$ and $(NH_4)_2S$ in the water nanodroplets, CdS was coupled with TiO_2 colloids.

3 Photocatalysis properties and applications

During the past decades, various photocatalysts have been reported, such as TiO_2, ZnO, WO_3, $ZnWO_4$, Bi_2WO_6, *etc.* The coupling of different semiconductors will result in improved photocatalytic activity. In type II heterostructure, excited electrons on the sensitizer semiconductor can transfer to the lower conduction band of the wide bandgap semiconductor, while holes are confined in sensitizer semiconductor, leading to an enhanced photocatalytic performance and an extended light absorption spectrum. Powdery photocatalysts have been a focus of great attention and development due to the high photocatalytic activity and relative simplicity of fabrication. However, powdery photocatalysts dispersed in solution agglomerate easily and are hard to separate from water. Recently, one-dimensional (1D) semiconductor nanostructures with type II core/shell structure grown on a substrate have made a profound impact on the application of photocatalysis. In this section, we review the photocatalytic properties of both powdery type II heterostructure photocatalysts and 1D type II core/shell structures grown on substrates based on very commonly used TiO_2 and ZnO material systems. Some others photocatalysts like $ZnWO_4$, Bi_2WO_6, α-Fe_2O_3, which have been intensively studied recently, are also presented. In particular, some type II structures which show high photocatalytic performance are highlighted.

3.1 Powdery photocatalysts

Photocatalysts are widely used in powdery form due to the high photocatalytic activity and relative simplicity of fabrication. A wide bandgap semiconductor is usually coated with a narrow bandgap semiconductor to form a type II heterostructure. As a result, the photoinduced charge separation efficiency and the solar energy utilization of semiconductor are greatly improved. The morphology and geometry of heterostructure, surface texture, and particle size of the sensitizer play important roles in interface charge transfer and photocatalytic performance.

3.1.1 TiO_2-based powdery type II heterostructures. TiO_2 photocatalyst is the most widely studied photocatalyst due to its high oxidative efficiency, photochemical stability, nontoxicity

and low-cost.[7–9] However, the high recombination ratios of photoinduced electron–hole pairs and poor response to visible light have hindered the application of TiO_2 in photocatalysis.[10,11] Coupling with a narrow bandgap semiconductor to form a type II heterostructure is an effective way to improve photocatalytic activity and extend the light adsorption spectrum of TiO_2. There has been much interest in this topic. Powdery TiO_2 type II heterostructures such as CdS/TiO_2,[24,74–78] $CdSe/TiO_2$[13] WS_2/TiO_2,[29] Bi_2S_3/TiO_2[79] have been reported. A chalcogenide with narrow bandgap is widely used as a photosensitizer to fabricate a TiO_2 based heterostructure and has received much attention. Taking a CdS/TiO_2 heterostructure as an example, CdS, with a bandgap of 2.25 eV, can be excited by visible light to generate electron–hole pairs, while TiO_2 can only function under the illumination of UV light. Since the CB position of CdS is higher than that of TiO_2, excited electrons on CdS can inject into TiO_2 while the holes remains in CdS as shown in Fig. 9.

Visible light generated electron transfer from CdS to TiO_2 can not only enhance the charge separation efficiency but also extend the spectral response. Liu and co-workers prepared CdS/TiO_2 semiconductor nanoparticles by microemulsion-mediated solvothermal hydrolyzation followed by acidic peptization of the precipitate. The photocatalytic activity of the CdS/TiO_2 photocatalyst was confirmed by methylene blue (MB) degradation under visible light irradiation ($\lambda > 420$ nm).[74] Yu and co-workers prepared nanosized CdS-sensitized TiO_2 nanocrystals *via* a microemulsion-mediated solvothermal method.[24] The morphologies of CdS/TiO_2 are shown in Fig. 10a and b. Compared with pure TiO_2, CdS/TiO_2 nanocrystals exhibit enhanced efficiency for decomposition of methylene blue under visible light irradiation (Fig. 10c). Formation of Ti^{3+} on TiO_2 under visible-light irradiation was demonstrated by electron paramagnetic resonance spectrum (EPR), indicating the effective photogenerated electron transfer from CB of CdS to that of TiO_2. They also synthesized a $CdSe/TiO_2$ heterostructured photocatalyst by an ultrasound-driven solution method.[13] The $CdSe/TiO_2$ heterostructured photocatalyst shows a higher photocatalytic activity than that of pure TiO_2 in the degradation of 4-chlorophenol under visible light irradiation ($\lambda > 400$ nm). The quantum size effect of CdSe plays an important role in enhancing charge separation efficiency and photocatalytic activity of the $CdSe/TiO_2$ heterostructured photocatalyst.[13] Moreover, MoS_2 and WS_2 nanocluster sensitized TiO_2 nanoparticles were synthesized *via in situ* photoreduction deposition by the same group.[29] The quantum confinement effects of MoS_2 and WS_2 can cause an appropriate alternation in the energy levels of the conduction and valence band edges, making them suitable for the photosensitization of visible light in a coupled semiconductor system. Compared with pure TiO_2, MoS_2/TiO_2 and WS_2/TiO_2 heterostructures show higher photocatalytic activity in MB and 4-chlorophenol degradation under visible light irradiation ($\lambda > 400$ nm).[29] Besides the chalcogenides, there are various narrow bandgap semiconductors that can be coupled with TiO_2 to form a type II heterostructure, enhancing photocatalytic performance and extending the light adsorption spectrum of TiO_2, such as Ag_2O,[80,81] $CuAlO_2$,[82] $LaVO_4$,[28] $AgIn_5S_8$,[83] V_2O_5.[84]

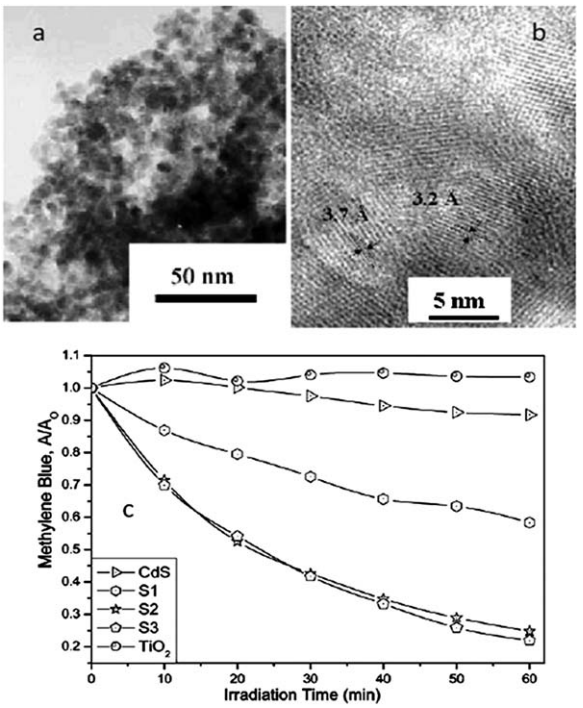

Fig. 10 (a and b) TEM and HRTEM images of CdS/TiO_2; (c) the MB degradation under visible light irradiation (660 nm) in the prepared photocatalysts (reprinted with permission from ref. 24, copyright 2003 Royal Society of Chemistry).

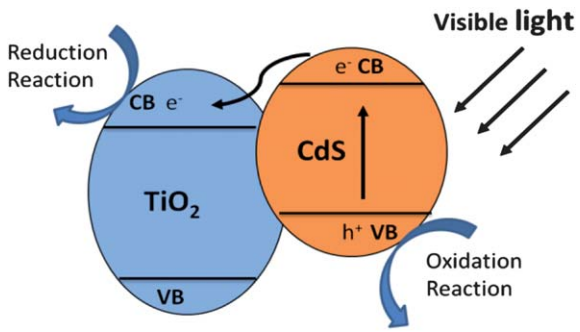

Fig. 9 Schematic illustration of charge transfer in CdS/TiO_2 heterostructure.

In addition, type II heterostructures can combine with another material to form ternary hybrid catalysts. For example, TiO_2 type II heterostructures usually combine with noble metals to enhance the photocatalytic activity in hydrogen production.[85] In the CdS/TiO_2/Pt system, the formation of the potential gradient at the interface between CdS and TiO_2 and the Pt fabrication method play important roles in determining the hydrogen production efficiency.[85]

3.1.2 ZnO-based powdery type II heterostructures. Although TiO_2 is the most widely employed photocatalyst, ZnO appears to be a suitable alternative to TiO_2. ZnO is also relatively inexpensive and its photodegradation mechanism is similar to that of TiO_2.[86] Moreover, some reports pointed out that ZnO exhibits a higher efficiency than TiO_2 in the photocatalytic degradation of some dyes in water.[87–89] Coupling with a narrow bandgap semiconductor is an effective way to enhance the

charge separation efficiency and improve the utilization of solar light of ZnO, such as C_3N_4,[25] ZnSe,[90] In_2O_3,[91] *etc.* Lee and co-workers synthesized three distinct type II ZnSe/ZnO heterostructures through simple solution-based surface modification reactions.[90] The morphologies of three distinct type ZnSe/ZnO heterostructures are shown in Fig. 11a. Compared with pure ZnO structure, these ZnSe/ZnO heterostructures showed higher photocatalytic activities in orange-II degradation under visible light irradiation (Fig. 11b). The group also investigated the effect of the morphologies and exposed crystal faces of ZnO on the photocatalytic activity. Yu and co-workers synthesized In_2O_3/ZnO heteronanostructures by a coprecipitation method.[91] The photocatalytic activity of In_2O_3/ZnO heterostructures was demonstrated to be higher than that of pure ZnO due to the enhanced charge separation and transport of the type II heterostructure. Different compositions and annealing temperatures affect the photocatalytic activities. The highest photocatalytic activity was obtained when annealing at 800 °C with a Zn/In ratio of 1 : 1. It is worth pointing out that ZnO has low stability under long reaction times due to photocorrosion, and some effort has been devoted to inhibiting photocorrosion.

Zhu and co-workers fabricated a type II graphite-like C_3N_4/ZnO heterostructure.[25] After coupling with C_3N_4, the photocurrent and photocatalytic activity of ZnO were both greatly enhanced under UV and visible light irradiation (Fig. 12a and b). Moreover, the photocorrosion of ZnO was successfully suppressed in the C_3N_4/ZnO heterostructure. The photocorrosion of ZnO is caused by photoinduced dissolution due to hole oxidation. Since the VB position of ZnO is lower than that of the C_3N_4, the photogenerated holes on ZnO could directly transfer to C_3N_4, leading to an effective photocorrosion inhibition (Fig. 12c). As shown in Fig. 12d, the visible photoactivity of C_3N_4/ZnO heterostructure originates from the injection of excited electrons from CB of C_3N_4 to the CB of ZnO.

3.1.3 Other powdery type II heterostructures. Besides TiO_2 and ZnO, there are also many other semiconductors with excellent photocatalytic properties that have been intensively studied recently, such as Fe_2O_3,[92,93] WO_3,[94] Bi_2WO_6,[27,95] $ZnWO_4$,[26,96] and $BiPO_4$.[97,98] $ZnWO_4$ has received considerable attention as UV light driven photocatalysts due to their relatively high activities for degradation of organic compounds.[26] It is important to develop novel methods for the improvement of the photocatalytic activity and solar energy utilization efficiency of

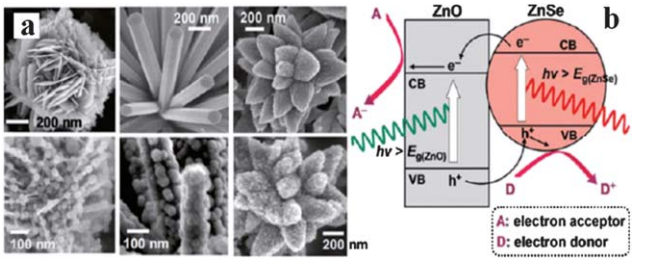

Fig. 11 (a) SEM images of ZnO/ZnSe heterostructures; (b) schematic diagram showing the energy band structures of a ZnO/ZnSe heterostructure (reprinted with permission from ref. 90, copyright 2011 American Chemical Society).

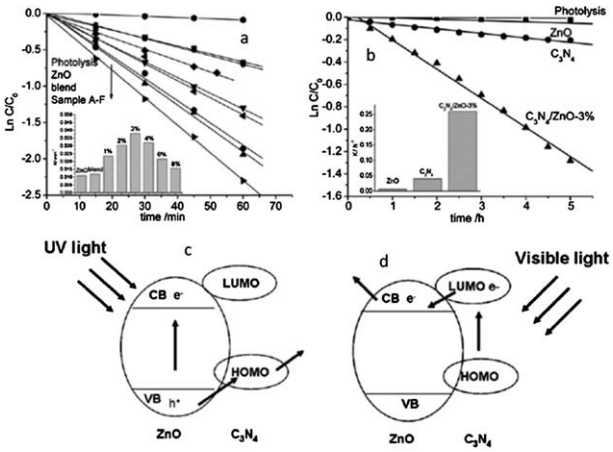

Fig. 12 Photocatalytic degradation of MB over ZnO and C_3N_4/ZnO photocatalysts: (a) under UV light irradiation and (b) under visible light irradiation (visible light region in the range of 400–800 nm; the main wavelength is about 550 nm); schematic drawing illustrating the mechanism of charge separation of C_3N_4/ZnO photocatalyst: (c) under UV light irradiation and (d) under visible light irradiation (reprinted with permission from ref. 25, copyright 2011 Royal Society of Chemistry).

$ZnWO_4$. Our group synthesized $ZnWO_4$ nanorods by a hydrothermal method,[26] and then prepared a $C_3N_4/ZnWO_4$ heterostructure *via* chemisorptions (Fig. 13a and b). As shown in Fig. 13c, a loading amount of 5% C_3N_4 over $ZnWO_4$ leads to an 80% increase in the photocatalytic activity under UV light irradiation. The enhanced UV light photocatalytic activity could be attributed to the high separation efficiency of the photogenerated charge pairs due to the type II heterostructure between C_3N_4 and $ZnWO_4$. Visible light activity of $C_3N_4/ZnWO_4$ was observed, which originated from the injection of excited electrons from the CB of C_3N_4 to the CB of $ZnWO_4$ (Fig. 13d).

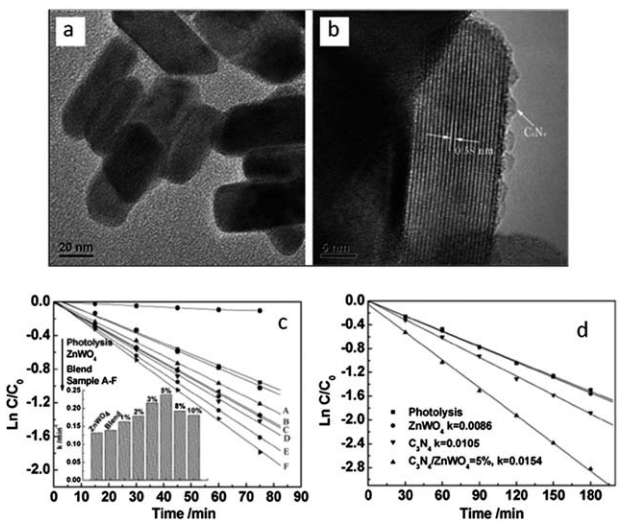

Fig. 13 The morphology of $ZnWO_4$ and $C_3N_4/ZnWO_4$ photocatalysts: (a) $ZnWO_4$ (b) $C_3N_4/ZnWO_4$; pseudo-first-order rates of MB degradation over $ZnWO_4$ and $C_3N_4/ZnWO_4$ photocatalysts: (c) under UV light irradiation (λ = 254 nm) (d) under visible light irradiation ($\lambda > 420$ nm) (reprinted with permission from ref. 26, copyright 2012 Royal Society of Chemistry).

$BiPO_4$ as an oxoacid salt photocatalyst has been reported to have an excellent photocatalytic activity under UV light irradiation. Zhu and co-workers fabricated a $C_3N_4/BiPO_4$ core/shell structure *via* an ultrasonic dispersion method.[98] After coupling with C_3N_4, the UV light photocatalytic activity of $BiPO_4$ was greatly enhanced and visible light photocatalytic activity was generated due to the type II structure. Recently, many new visible-light-active photocatalysts have been reported to have good photocatalytic performance, such as Bi_2WO_6,[27,95] $BiVO_4$,[99] and $InVO_4$.[100] The formation of type II structure is also an effective way to enhance the photocatalytic activity of visible-light-active photocatalysts. It has been reported that a C_3N_4/Bi_2WO_6 photocatalyst has higher photocatalytic activity than that of pure Bi_2WO_6.[27] The enhanced photocatalytic activity of the C_3N_4/Bi_2WO_6 photocatalyst could be attributed to the enhanced charge separation efficiency due to the type II structure. A Bi_2S_3/Bi_2WO_6 heterostructure was prepared to overcome the drawback of low photocatalytic efficiency and narrow photoresponse range of Bi_2WO_6.[101] The Bi_2S_3/Bi_2WO_6 heterostructure possesses a wide photoabsorption until 800 nm and shows a higher photocatalytic activity for phenol degradation than that of pure Bi_2WO_6.

3.2 1D type II core/shell photocatalysts

Compared with powder photocatalysts, one-dimensional (1D) semiconductor nanostructures with type II core/shell structures grown on substrates have made a profound impact on the application of photocatalysts because they effectively avoid agglomeration and possess a direct electrical pathway for the rapid transport of photogenerated carriers to the photoelectrode.[102–104] The core is usually coated with a uniform shell and consequently a large interfacial area is formed in the interlayer, which ensures rapid charge separation. As a result, the nonradiative recombination of the electrons with electrolyte is inhibited and corrosion of core nanowires is prevented from electrolyte.[105] Sometimes, the shell is substituted by quantum dots, which has been confirmed as a promising alternative to photosensitive dyes.[106] They can produce multiple electron–hole pairs per photon and thus enhance the photoconversion efficiency.[107]

3.2.1 TiO_2-based type II core/shell structure nanowire arrays. Compared with TiO_2 film, TiO_2 nanowire arrays have larger surface area, which improves the light absorption efficiency. After decoration with small bandgap semiconductor quantum dots, the light absorption efficiency is further enhanced. For example, the formation of CdS quantum dots on vertically aligned TiO_2 nanorods make the photocurrent of the composite 28.6 times higher than that of a pure TiO_2 nanorod array.[108] In addition, Li and co-workers demonstrated that a CdS quantum dot-decorated TiO_2 nanowire array showed an enhanced photoactivity in the entire wavelength region from 350 to 550 nm.[109] Similar improved photoelectrochemical performance has also been achieved on a CdS nanoparticle-sensitized TiO_2 nanorod array grown by a hydrothermal method.[110]

Significantly, Yang and co-workers synthesized *Z*-scheme type $CdS/Au/TiO_2$ hollow nanorod arrays (THNAs) on glass substrates by co-modifying TiO_2 nanorods with Au and CdS nanoparticles.[111] Ultraviolet-visible absorption spectra showed a red shift to 585 nm due to the strong electromagnetic coupling of Au and CdS compared with the pure TiO_2 nanorod arrays and single Au or CdS nanoparticles. The CdS/Au/THNAs three-component nanojunction also exhibited enhanced photocatalytic activity. Using this kind of three-component nanojunction photocatalyst, the content of MB reduced by 72% after 2 h which is much more than that (15%) of pure THNAs under the same conditions.

Some ternary compounds are also used to modify TiO_2 to get continuously adjustable spectral absorption by controlling the components. Park and co-workers reported that the TiO_2 nanocable arrays coated by an Se-rich composition (CdS/CdSSe/CdSe multishell structures) showed excellent solar photocurrents and hydrogen generation rates.[112] They also studied the photoelectric conversion efficiency of samples shelled with different compositions. It was confirmed that the CdS/CdSSe/CdSe multishell structures gained higher photoelectric conversion efficiency than that of CdSe and CdS.

In addition to TiO_2 nanowire arrays, TiO_2 nanotube arrays have also been used for type II band structures by decorating with CdS (ref. 113) and $SrTiO_3$.[114] Lin and co-workers used free-standing open-ended TiO_2 nanotube membranes to degrade RhB, and then fabricated compound nanocables by stuffing the membrane with CdS.[113] Fig. 14 shows the setup used for flow-through photocatalysis experiments and the way in which the CdS is loaded. CdS/TiO_2 nanocomposites show higher photocatalytic degradation activity compared with that of bare TiO_2 nanotubes. The results suggest that the load of CdS increases light absorption of the CdS/TiO_2 nanocomposites and, meanwhile, enhances the carrier separation efficiency. Furthermore, N and F codoped TiO_2 nanotube arrays coupled with PbO nanoparticles showed significant enhancement on the photocatalytic degradation of organic pollutants due to the opto-electronic cooperation between TiO_2 and PbO.[115] Also, based on the same mechanism, this enhanced photocatalytic degradation has been realized with a CdSe nanoparticle-decorated TiO_2 nanotube array.[116]

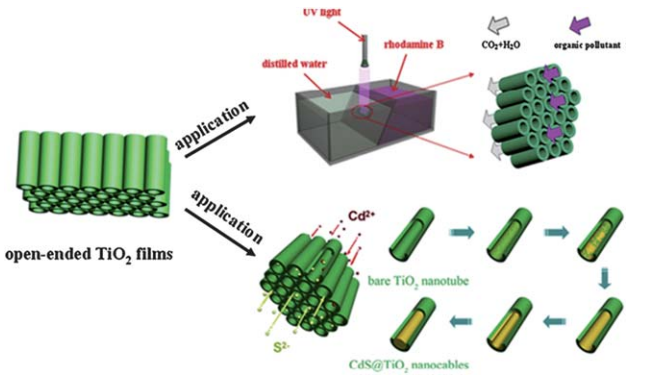

Fig. 14 Schematic of applications of free-standing open-ended TiO_2 nanotube membranes (reprinted with permission from ref. 113, copyright 2012 Elsevier).

Furthermore, compared with single shell nanostructures, double-shell TiO_2 nanostructures further improve photoelectrochemical (PEC) properties, as reported by Xiao and coworkers.[117] Cu_2O could absorb a wide range of visible light due to its narrow band gap (<2 eV), but it's difficult to use for water splitting due to its weak stability in solution. Xiao and coworkers prepared TiO_2/CuO/Cu_2O nanowire arrays on Au-coated copper substrates through controlled air annealing of the electrodeposited Cu nanowires and then dip coating with TiO_2. The step-by-step enhancement of charge separation efficiency is indicated in the electrochemical impedance spectra (EIS) data in Fig.15a. Fig. 15b shows the energy band diagram of TiO_2/CuO/Cu_2O nanowire arrays and also the charge transfer route in electrolyte solution.

3.2.2 ZnO-based type II core/shell nanowire arrays. Compared with TiO_2, ZnO possesses a higher electron mobility and longer photoexcited electron lifetime.[118] Thus, it is considered as a promising alternative to TiO_2. Indeed, coupling with a small bandgap semiconductor quantum dots, ZnO-based type II core/shell nanowire array photocatalysts have shown high-performance photocatalytic properties. For example, significant photocurrent and efficiency were obtained on a ZnO nanowire array sensitized by CdTe quantum dots.[32] This is because a type II core/shell structure was formed by coating the CdTe quantum dots on the ZnO nanowires. In addition, the stability of the overall water-splitting reaction was increased because the employment of CdTe avoided anodic decomposition and corrosion. Therefore, the electrochemical reaction performance was enhanced. The photoconversion efficiency (1.83%) was more than 200% higher than that of pristine ZnO nanowires. Similarly, a CdS nanoparticle/ZnO nanowire array also showed enhanced photocurrent characteristics compared with the photoelectrode cell of a bare ZnO nanowire array, owing to their higher visible-light absorption capability and charge carrier transfer efficiency.[30,31] An Al-doped ZnO nanorod array decorated with PbS nanoparticles also showed excellent photocatalytic properties.[119]

Recently, highly efficient photoelectrochemical hydrogen generation has been demonstrated on hierarchical WO_x/ZnO nanowires by cosensitizing CdSe and CdS as shown in Fig. 16a.[120] The support of the CdSe shell and CdS nanoparticles extended the light absorption of the WO_x/ZnO nanowire array to a wavelength of 800 nm. A photocurrent density as high as 11 mA cm^{-2} at −0.5 V (*vs.* SCE) under 1.5 AM irradiation was achieved. This kind of enhanced light harvesting is obviously attributed to the synergy between WO_x/ZnO and CdSe/CdS as well as the formation of type II core/shell structure. Fig. 16b and c show current density of CdSe/CdS/WO_x/ZnO under chopped illumination.

In addition to quantum dots, a more commonly used decoration is the uniform nanoscale shell. For example, a ZnO nanowire array coated with a CdTe shell demonstrated a photocurrent density of ~5.9 mA cm^{-2} under visible light illumination of 100 mW cm^{-2} at zero bias potential. The authors suggested that the favorable absorption of CdTe and the type II band alignment contributed to the excellent performance of this photoelectrode.[48] Furthermore, our group recently successfully fabricated ZnS_xSe_{1-x}/ZnO core/shell nanowires *via* a two-step CVD method. The obtained core/shell structure showed a significant improvement of visible light absorption efficiency. It was explicitly demonstrated that the introduction of a ZnS_xSe_{1-x} shell to ZnO nanowires profoundly improved the photogenerated charge separation process.[44]

Based on the similar mechanism, there are also other 1D core/shell examples like CdSSe/ZnO.[50] However, these works paid more attention to the manipulation of electronic structure. One method is to tailor the composition of the shell through controlling the synthetic process, and thus a tunable band gap can be achieved, which results in the continuous absorption of the solar spectrum. For example, $Zn_xCd_{1-x}Se$/ZnO core/shell nanowire arrays which were synthesized by temperature-gradient CVD yielded a continuous absorption edge from 2.7 to 1.77 eV across the sample surface by adjusting the Zn composition.[35] This core/shell nanowire array showed photocurrent density of ~5.6 mA cm^{-2} under 1 sun solar light illumination at zero bias *versus* Ag/AgCl. Another example is the $Zn_xCd_{1-x}S$/ZnO core/shell nanorod array whose shell also showed a tunable band gap from 2.52 to 3.11 eV.[47] They exhibited a high photocatalytic activity and good stability in the degradation of the methylorange.

Another method is to change the element ratio of the intermediate layer so that exciton generation and separation were facilitated. For example, due to the formation of a CdZnSSe intermediate layer, CdSSe/ZnO core/shell nanowire showed

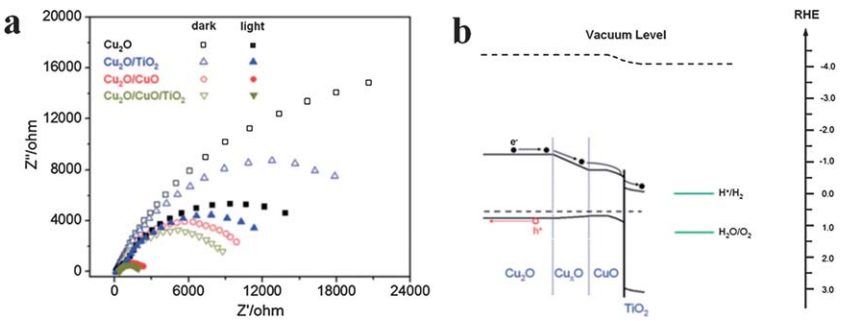

Fig. 15 (a) EIS data of Cu_2O, Cu_2O/CuO and Cu_2O/CuO/TiO_2 nanowire array based photocathodes both in the dark and under light; (b) energy band diagram and charge transfer for Cu_2O/CuO/TiO_2 (reprinted with permission from ref. 117, copyright 2013 Royal Society of Chemistry).

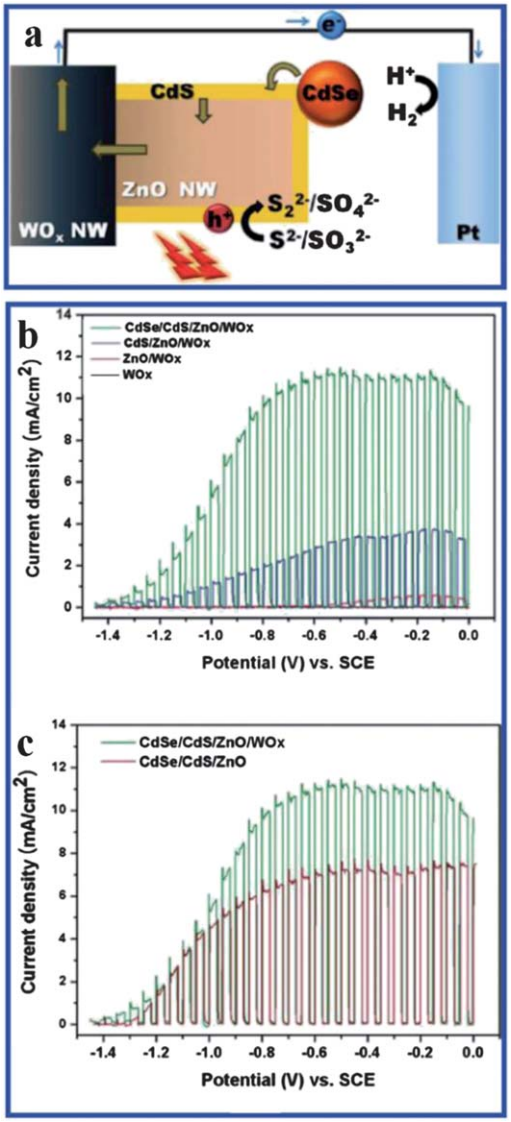

Fig. 16 (a) Schematic of the photoelectrochemical hydrogen generation system based on CdSe/CdS/WO_x/ZnO; (b) current density as a function of potential under chopped illumination (100 mW cm^{-2}) of (black) as-prepared WO_x nanowhiskers, (red) WO_x/ZnO, (blue) CdS/WO_x/ZnO, and (green) CdSe/CdS/WO_x/ZnO; (c) comparison of *J–E* curves of CdSe/CdS/WO_x/ZnO and CdSe/CdS/ZnO under chopped illumination (reprinted with permission from ref. 120, copyright 2011 American Chemical Society).

higher photocurrent and hydrogen generation rate than that of CdS/TiO_2 under AM 1.5 G conditions.[50] The authors believe that Zn containing alloy layers in the interface region improved the epitaxial growth of single-crystalline shell layers on the ZnO nanowire core by the way of reducing the lattice mismatch and the number of defect sites.

Some other narrow band gap semiconductor materials, such as V_2O_5 whose band gap is 2.2 eV covering visible light range, have also been used to decorate ZnO.[121] In the example of a V_2O_5-sensitized ZnO nanowire array, a ZnO nanowire array was first synthesized by a hydrothermal growth process, and then coated with V_2O_5 by magnetron sputtering. The absorption edge of the V_2O_5/ZnO core/shell structure was longer than that of pure ZnO nanowires. In addition, after annealing, the absorption of UV became weak while visible light absorption was enhanced due to the low diffusion of Zn atoms into the V_2O_5 layer. To further improve photoelectrochemical hydrogen generation, a double-shell structure such as CdSe/CdS has been used to decorate ZnO nanowire arrays.[122] This fabrication lengthens the absorbance spectra of ZnO NWs array to 700 nm. The PEC performance of pure ZnO NWs, CdS/ZnO NWs, CdSe/CdS/ZnO NWs also demonstrated a step by step enhancement.

3.2.3 Other kinds of nanowire array-based type II core/shell heterostructures. Recently, α-Fe_2O_3 has been widely explored as photocatalyst due to its favorable optical band gap (2.1 eV), natural abundance, low cost, and good chemical stability.[123,124] However, its practical applications are limited because of its small absorption coefficient and the low carrier mobility. To solve this problem, Feng and co-workers constructed a type II heterojunction between α-Fe_2O_3 and $BiV_{1-x}Mo_xO_4$. A graphene sheet, which has excellent charge carrier mobility, was utilized as the electron mediator. The $BiV_{1-x}Mo_xO_4$/graphene/α-Fe_2O_3 core/shell heterojunction array yielded a pronounced photocurrent density of ~1.97 mA cm^{-2} at 1.0 V *vs.* Ag/AgCl and a high photoconversion efficiency of ~0.53% at −0.04 V *vs.* Ag/AgCl under the irradiation of a Xe lamp as shown in Fig. 17c and d.[34] This demonstrated that the graphene sheet behaves as an electron and hole conductor, which accelerated the electron–hole separation as shown in Fig. 17b. Fig. 17a is the top view SEM image of $BiV_{1-x}Mo_xO_4$/graphene/α-Fe_2O_3 core/shell.

In visible light driven photocatalytic systems, Si nanowire was also used as the core owing to its relatively high conduction band and valence band. Semiconductor materials with wide bandgap were used as the shell, such as TiO_2,[125,126] ZnO,[127] ZnSe.[128] As discussed in Xie's work, p-Si nanowires/TiO_2 heterojunction arrays as the photocathode could utilize the visible

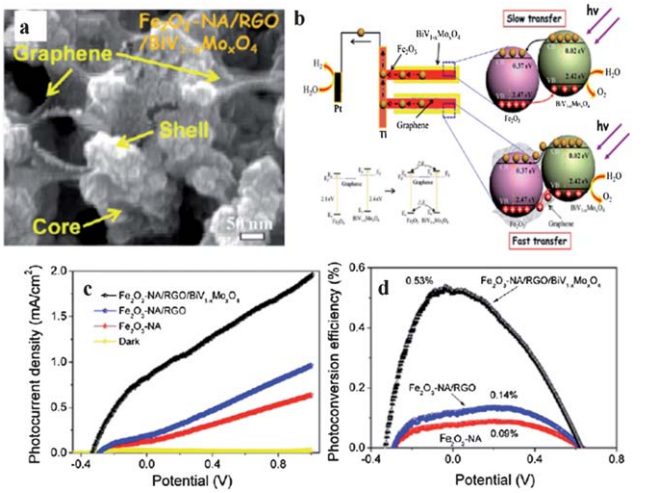

Fig. 17 (a) Top SEM image of $BiV_{1-x}Mo_xO_4$/graphene/α-Fe_2O_3 core/shell; (b) schematic of energy band structure of $BiV_{1-x}Mo_xO_4$/graphene/α-Fe_2O_3 core/shell; (c) potential-dependent photocurrent density and (d) photoconversion efficiency as a function of applied potential of α-Fe_2O_3, RGO/α-Fe_2O_3, $BiV_{1-x}Mo_xO_4$/graphene/α-Fe_2O_3 (reprinted with permission from ref. 34, copyright 2012 American Chemical Society).

light including wavelengths longer than 600 nm.[125] They used p-Si as the under-layer to construct a p–n heterojunction with n-type TiO_2 so that the semiconductors with narrow band gap could capture most of the sunlight photons to generate more photoelectrons for pollutant decomposition. The results show that the degradation efficiency of phenol reached 80.7% in 100 min under visible light owing to the synergy between the electrochemical process and the photocatalytic process. Later, Wang and co-workers demonstrated a mace-like core/shell three-dimensional (3D) nanorod network. In this network, the core array is composed of Si nanowires and the TiO_2 nanorods were grown vertically on the frame.[126] This unique structure gained a PEC efficiency of 2.1% which is three times higher than that of the TiO_2 film/Si nanowire structure.

Based on a similar principle, Chen and co-workers obtained ZnO/Si core/shell nanowire arrays with about 8% optical reflectance in the visible region, which results in good optical absorption.[127] They also studied the water splitting performance of ZnO/Si nanowire arrays. It was confirmed that the ZnO/Si core/shell nanowire arrays achieved higher photoconversion efficiency than that of the planar bilayer structure of ZnO/Si and the pure planar ZnO. In addition, p-type Si nanowire arrays coated with ZnSe nanoparticles also exhibited enhanced photodetection and photocatalytic performances.[128]

4 Conclusions

Photocatalysis appears to be a promising way to solve environmental and energy issues in the future. Over the past few decades, continuous breakthroughs in the synthesis, modification and application of semiconductors have been reported. In this review, we have described the general strategies and recent progress in the fabrication of type II heterostructures for environmental remediation and water splitting. We focus on synthetic methods and photocatalytic properties of TiO_2 and ZnO based visible light driven type II 0D and 1D heterostructured photocatalysts. Some other low dimensional nanomaterials which showed high-performance photocatalysis are also presented, such as $ZnWO_4$ nanoparticles, Bi_2WO_6 nanoparticles, α-Fe_2O_3 nanowire arrays and p-Si nanowire arrays. The formation of a type II heterostructure that integrates multiple functional components in the nanoscale significantly enhances the photocatalytic performance, which arises from: (1) the synergy of absorption between the core and the sensitizer; (2) type II heterostructures promote separation and transformation efficiency of photogenerated electron–hole pairs.

It is worth noting that although great progress has achieved in the study of type II heterostructured photocatalysts, extensive application of type II heterostructured photocatalysts still faces several tough challenges: firstly, the quantum efficiency of type II heterostructures is still too low to utilize solar energy with high efficiency. Thus the dynamic behaviour of photogenerated carriers in the interface and surface of type II heterostructure needs to be further clarified so that researchers can design type II heterostructures rationally. Moreover, despite the successfully use of various synthetic methods to prepare type II nanoscale heterostructured photocatalysts, production by these methods is far from sufficient for industrial applications. In addition, type II heterostructured nanomaterials still suffer from chemical instability, which severely decreases the efficiency of the photocatalysts. Even the safety and the secondary pollution to the environment of nanoscale photocatalysts are still ambiguous. All in all, researchers all around the world need to carry out systematic and careful experimental studies and thus establish general and rational design guidelines in fabricating type II heterostructured nanoscale photocatalysts.

Acknowledgements

This work was supported by the 973 Program of Ministry of Science and Technology of China (no. 2012CB934103) and the 100-Talents Program of the Chinese Academy of Sciences (no. Y1172911ZX).

Notes and references

1 R. J. Cambell, *China and the United States—A comparison of green energy programs and policies. Congressional Research Service. Report for Congress*, Washington, DC, 2011.
2 A. Fujishima and K. Honda, *Nature*, 1972, **238**, 37–38.
3 M. R. Hoffmann, S. T. Martin, W. Choi and D. W. Bahnemann, *Chem. Rev.*, 1995, **95**, 69–96.
4 H. Zhou, Y. Qu, T. Zeid and X. Duan, *Energy Environ. Sci.*, 2012, **5**, 6732–6743.
5 I. K. Konstantinou and T. A. Albanis, *Appl. Catal., B*, 2004, **49**, 1–14.
6 M. G. Walter, E. L. Warren, J. R. McKone, S. W. Boettcher, Q. Mi, E. A. Santori and N. S. Lewis, *Chem. Rev.*, 2010, **110**, 6446–6473.
7 A. Fujishima, T. N. Rao and D. A. Tryk, *J. Photochem. Photobiol., C*, 2000, **1**, 1–21.
8 K. I. Hadjiivanov and D. G. Klissurski, *Chem. Soc. Rev.*, 1996, **25**, 61–69.
9 A. Heller, *Acc. Chem. Res.*, 1995, **28**, 503–508.
10 H. Kominami, S. Murakami, J. Kato, Y. Kera and B. Ohtani, *J. Phys. Chem. B*, 2002, **106**, 10501–10507.
11 J. C. Yu, L. Z. Zhang, Z. Zheng and J. C. Zhao, *Chem. Mater.*, 2003, **15**, 2280–2286.
12 R. Wang, G. Jiang, Y. Ding, Y. Wang, X. Sun, X. Wang and W. Chen, *ACS Appl. Mater. Interfaces*, 2011, **3**, 4154–4158.
13 W. Ho and J. C. Yu, *J. Mol. Catal. A: Chem.*, 2006, **247**, 268–274.
14 B. Kraeutler and A. J. Bard, *J. Am. Chem. Soc.*, 1978, **100**, 4317–4318.
15 V. Subramanian, E. E. Wolf and P. V. Kamat, *J. Am. Chem. Soc.*, 2004, **126**, 4943–4950.
16 R. Asahi, T. Morikawa, T. Ohwaki, K. Aoki and Y. Taga, *Science*, 2001, **293**, 269–271.
17 P. V. Kamat, *Pure Appl. Chem.*, 2002, **74**, 1693–1706.
18 Y. Wang, R. Shi, J. Lin and Y. Zhu, *Appl. Catal., B*, 2010, **100**, 179–183.
19 Y. Wang, J. Xu, W. Zong and Y. Zhu, *J. Solid State Chem.*, 2011, **184**, 1433–1438.

20 Y. Wang, J. Lin, R. Zong, J. He and Y. Zhu, *J. Mol. Catal. A: Chem.*, 2011, **349**, 13–19.
21 H. McDaniel, P. E. Heil, C. L. Tsai, K. K. Kim and M. Shim, *ACS Nano*, 2011, **5**, 7677–7683.
22 M. Shim, H. McDaniel and N. Oh, *J. Phys. Chem. Lett.*, 2011, **2**, 2722–2727.
23 A. Kudo and Y. Miseki, *Chem. Soc. Rev.*, 2009, **38**, 253–278.
24 J. C. Yu, L. Wu, J. Lin, P. Lia and Q. Li, *Chem. Commun.*, 2003, 1552–1553.
25 Y. Wang, R. Shi, J. Lin and Y. Zhu, *Energy Environ. Sci.*, 2011, **4**, 2922–2929.
26 Y. Wang, Z. Wang, S. Muhammad and J. He, *CrystEngComm*, 2012, **14**, 5065–5070.
27 Y. Wang, X. Bai, C. Pan, J. He and Y. Zhu, *J. Mater. Chem.*, 2012, **22**, 11568–11573.
28 H. Huang, D. Li, Q. Lin, W. Zhang, Y. Shao, Y. Chen, M. Sun and X. Fu, *Environ. Sci. Technol.*, 2009, **43**, 4164–4168.
29 W. Ho, J. C. Yu, J. Lin, J. Yu and P. Li, *Langmuir*, 2004, **20**, 5865–5869.
30 Y. Tak, H. Kim, D. Lee and K. Yong, *Chem. Commun.*, 2008, 4585–4587.
31 Y. Tak, S. J. Hong, J. S. Lee and K. Yong, *Cryst. Growth Des.*, 2009, **9**, 2627–2632.
32 H. M. Chen, C. K. Chen, Y. C. Chang, C. W. Tsai, R. S. Liu, S. F. Hu, W. S. Chang and K. H. Chen, *Angew. Chem.*, 2010, **122**, 6102–6105.
33 J. Johansson and K. A. Dick, *CrystEngComm*, 2011, **13**, 7175–7184.
34 Y. Hou, F. Zuo, A. Dagg and P. Feng, *Nano Lett.*, 2012, **12**, 6464–6473.
35 H. Li, C. Cheng, X. Li, J. Liu, C. Guan, Y. Y. Tay and H. J. Fan, *J. Phys. Chem. C*, 2012, **116**, 3802–3807.
36 J. Li, M. W. G. Hoffmann, H. Shen, C. Fabrega, J. D. Prades, T. Andreu, F. Hernandez-Ramirezbc and S. Mathur, *J. Mater. Chem.*, 2012, **22**, 20472–20476.
37 J. Luo, L. Ma, T. He, C. F. Ng, S. Wang, H. Sun and H. J. Fan, *J. Phys. Chem. C*, 2012, **116**, 11956–11963.
38 X. Wang, L. Yin, G. Liu, L. Wang, R. Saito, G. Q. M. Lu and H. M. Cheng, *Energy Environ. Sci.*, 2011, **4**, 3976–3979.
39 X. Liu, C. Wang, X. Xu, J. Xu, X. Chen, X. Liu, R. Zou and H. Xing, *CrystEngComm*, 2013, **15**, 1139–1145.
40 S. Cho, J. W. Jang, J. S. Lee and K. H. Lee, *Nanoscale*, 2012, **4**, 2066–2071.
41 J. Schrier, D. O. Demchenko and L. W. Wang, *Nano Lett.*, 2007, **7**, 2377–2382.
42 Z. Yin, Z. Wang, Y. Du, X. Qi, Y. Huang, C. Xue and H. Zhang, *Adv. Mater.*, 2012, **24**, 5374–5378.
43 A. Kar, S. Kundu and A. Patra, *RSC Adv.*, 2012, 10222–10230.
44 Z. Wang, X. Zhan, Y. Wang, M. Safdar, M. Niu, J. Zhang, Y. Huang and J. He, *Appl. Phys. Lett.*, 2012, **101**, 073105.
45 H. Jia, H. Xu, Y. Hu, Y. Tang and L. Zhang, *Electrochem. Commun.*, 2007, **9**, 354–360.
46 Z. Lu, J. Xu, X. Xie, H. Wang, C. Wang, S.-Y. Kwok, T. Wong, H. L. Kwong, I. Bello, C. S. Lee, S. T. Lee and W. Zhang, *J. Phys. Chem. C*, 2012, **116**, 2656–2661.
47 S. Xie, X. Lu, T. Zhai, J. Gan, W. Li, M. Xu, M. Yu, Y. M. Zhang and Y. Tong, *Langmuir*, 2012, **28**, 10558–10564.
48 X. Wang, H. Zhu, Y. Xu and H. Wang, *ACS Nano*, 2010, **4**, 3302–3308.
49 M. Lee and K. Yong, *Nanotechnology*, 2012, **23**, 1–7.
50 Y. Myung, D. M. Jang, T. K. Sung, Y. J. Sohn, G. B. Jung, Y. J. Cho, H. S. Kim and J. Park, *ACS Nano*, 2010, **4**, 3789–3800.
51 Z. Wang, H. Yin, C. Jiang, M. Safdar and J. He, *Appl. Phys. Lett.*, 2012, **101**, 253109.
52 M. Zhong, Y. Li, I. Yamada and J. J. Delaunay, *Nanoscale*, 2012, **4**, 1509–1514.
53 M. Zhong, Y. Li, T. Tokizono, M. Zheng, I. Yamada and J. J. Delaunay, *J. Nanopart. Res.*, 2012, **14**, 804–814.
54 H. Y. Chao, J. H. Cheng, J. Y. Lu, Y. H. Chang, C. L. Cheng and Y. F. Chen, *Superlattices Microstruct.*, 2010, **47**, 160–164.
55 R. S. Mane and C. D. Lokhande, *Mater. Chem. Phys.*, 2000, **65**, 1–31.
56 R. Ghosh Chaudhuri and S. Paria, *Chem. Rev.*, 2011, **112**, 2373–2433.
57 X. Fang, T. Zhai, U. K. Gautam, L. Li, L. Wu, Y. Bando and D. Golberg, *Prog. Mater. Sci.*, 2011, **56**, 175–287.
58 A. Datta, S. K. Panda and S. Chaudhuri, *J. Phys. Chem. C*, 2007, **111**, 17260–17264.
59 S. Zhao, S. Chen, H. Yu and X. Quan, *Sep. Purif. Technol.*, 2012, **99**, 50–54.
60 C. Z. Yao, B. H. Wei, L. X. Meng, H. Li, Q. J. Gong, H. Sun, H. X. Ma and X. H. Hu, *J. Power Sources*, 2012, **207**, 222–228.
61 B. Sun, Y. Z. Hao, F. Guo, Y. Cao, Y. Zhang, Y. Li and D. Xu, *J. Phys. Chem. C*, 2011, **116**, 1395–1400.
62 X. Zhou, B. Jin, L. Li, F. Peng, H. Wang, H. Yub and Y. Fang, *J. Mater. Chem.*, 2012, **22**, 17900–17905.
63 H. Wang, T. Wang, X. Wang, R. Liu, B. Wang, H. Wang, Y. Xu, J. Zhang and J. Duan, *J. Mater. Chem.*, 2012, **22**, 12532–12537.
64 J. B. Wu, Z. G. Li, X. H. Huang and Y. Lin, *J. Power Sources*, 2013, **224**, 1–5.
65 M. Y. Chen and Y. J. Hsu, *Nanoscale*, 2013, **5**, 363–368.
66 L. Dloczik and R. Konenkamp, *Nano Lett.*, 2003, **3**, 651–653.
67 S. Khanchandani, S. Kundu, A. Patra and A. K. Ganguli, *J. Phys. Chem. C*, 2012, **116**, 23653–23662.
68 Y. F. Nicolau, *Appl. Surf. Sci.*, 1985, **22/23**, 1061–1074.
69 B. Mukherjee, A. Peterson and V. R. Subramanian, *Chem. Commun.*, 2012, **48**, 2415–2417.
70 W. Ho and J. C. Yu, *J. Mol. Catal. A: Chem.*, 2006, **247**, 268–274.
71 M. T. Uddin, Y. Nicolas, C. L. Olivier, T. Toupance, L. Servant, M. M. Muller, H. Kleebe, J. Ziegler and W. Jaegermann, *Inorg. Chem.*, 2012, **51**, 7764–7773.
72 K. Li, B. Chai, T. Peng, J. Mao and L. Zan, *ACS Catal.*, 2013, **3**, 170–177.
73 A. Kar, S. Kundu and A. Patra, *RSC Adv.*, 2012, **2**, 10222–10230.
74 J. Wang, Z. Liu, Q. Zheng, Z. He and R. Cai, *Nanotechnology*, 2006, **17**, 4561–4566.
75 H. L. Meng, C. Cui, H. L. Shen, D. Y. Liang, Y. Z. Xue, P. G. Li and W. H. Tang, *J. Alloys Compd.*, 2012, **527**, 30–35.
76 A. Fujishima, X. Zhang and D. A. Tryk, *Surf. Sci. Rep.*, 2008, **63**, 515–582.

77 J. S. Jang, S. H. Choi, H. G. Kim and J. S. Lee, *J. Phys. Chem. C*, 2008, **112**, 17200–17250.
78 J. C. Yu, L. Wu, J. Lin, P. Li and Q. Li, *Chem. Commun.*, 2003, 1552–1553.
79 Y. Bessekhouad, D. Robert and J. V. Weber, *J. Photochem. Photobiol., A*, 2004, **163**, 569–580.
80 W. Zhou, H. Liu, J. Wang, D. Liu, G. Du, S. Han, J. Lin and R. Wang, *Phys. Chem. Chem. Phys.*, 2010, **12**, 15119–15123.
81 D. Sarkar, C. K. Ghosh, S. Mukherjee and K. K. Chattopadhyay, *ACS Appl. Mater. Interfaces*, 2012, **5**, 331–337.
82 R. Brahimi, Y. Bessekhouad, A. Bouguelia and M. Trari, *J. Photochem. Photobiol., A*, 2007, **186**, 242–247.
83 K. Li, B. Chai, T. Peng, J. Mao and L. Zan, *ACS Catal.*, 2013, **3**, 170–177.
84 Y. Wang, Y. R. Su, L. Qiao, L. X. Liu, Q. Su, C. Q. Zhu and X. Q. Liu, *Nanotechnology*, 2011, **22**, 225702–225709.
85 H. Park, W. Choi and M. R. Hoffmann, *J. Mater. Chem.*, 2008, **18**, 2379.
86 B. Dindar and S. Icli, *J. Photochem. Photobiol., A*, 2001, **140**, 263–268.
87 C. Lizama, J. Freer, J. Baeza and H. D. Mansilla, *Catal. Today*, 2002, **76**, 235–246.
88 A. A. Khodja, T. Sehili, J. Pilichowski and P. Boule, *J. Photochem. Photobiol., A*, 2001, **141**, 231–239.
89 C. Ye, Y. Bando, G. Shen and D. Golberg, *J. Phys. Chem. B*, 2006, **110**, 15146–15151.
90 S. Cho, J. W. Jang, J. Kim, J. S. Lee, W. Choi and K. H. Lee, *Langmuir*, 2011, **27**, 10243–10250.
91 Z. Wang, B. Huang, Y. Dai, X. Qin, X. Zhang, P. Wang, H. Liu and J. Yu, *J. Phys. Chem. C*, 2009, **113**, 4612–4617.
92 J. S. Jang, J. Lee, H. Ye, F. F. Fan and A. J. Bard, *J. Phys. Chem. C*, 2009, **113**, 6719–6724.
93 L. Li, Y. Chu, Y. Liu and L. Dong, *J. Phys. Chem. C*, 2007, **111**, 2123–2127.
94 R. Abe, T. Takata, H. Sugihara and K. Domen, *Chem. Commun.*, 2005, 3829–3831.
95 A. Kudo and S. Hijii, *Chem. Lett.*, 1999, 1103–1104.
96 R. Shi, Y. Wang, D. Li, J. Xu and Y. Zhu, *Appl. Catal., B*, 2010, **100**, 173–178.
97 C. Pan and Y. Zhu, *Environ. Sci. Technol.*, 2010, **44**, 5570–5574.
98 C. Pan, J. Xu, Y. Wang, D. Li and Y. Zhu, *Adv. Funct. Mater.*, 2012, **22**, 1518–1524.
99 J. Yu and A. Kudo, *Adv. Funct. Mater.*, 2006, **16**, 2163–2169.
100 J. Ye, Z. Zou, M. Oshikiri, A. Matsushita, M. Shimoda, M. Imai and T. Shishido, *Chem. Phys. Lett.*, 2002, **356**, 221–226.
101 Z. Zhang, W. Wang, L. Wang and S. Sun, *ACS Appl. Mater. Interfaces*, 2012, **4**, 593–597.
102 L. J. Lauhon, M. S. Gudiksen, D. Wang and C. M. Lieber, *Nature*, 2002, **420**, 57–61.
103 N. Skold, L. S. Karlsson, M. W. Larsson, M. E. Pistol, W. Seifert, J. Tragardh and L. Samuelson, *Nano Lett.*, 2005, **5**, 1943–1947.
104 Y. Zhang, L. W. Wan and A. Mascarenhas, *Nano Lett.*, 2007, **7**, 1264–1269.
105 M. Seol, H. Kim, Y. Tak and K. Yong, *Chem. Commun.*, 2010, **46**, 5521–5523.
106 A. J. Nozik, *Physica E*, 2002, **14**, 115–120.
107 J. E. Murphy, M. C. Beard, A. G. Norman, S. P. Ahrenkiel, J. C. Johnson, P. Yu, O. I. Micic, A. J. Nozik, R. J. Ellingson and A. J. Nozik, *J. Am. Chem. Soc.*, 2006, **128**, 3241–3247.
108 H. Wang, Y. Bai, H. Zhang, Z. Zhang, J. Li and L. Guo, *J. Phys. Chem. C*, 2010, **114**, 16451–16455.
109 H. Wang, G. Wang, Y. Ling, M. Lepert, C. Wang, J. Z. Zhanga and Y. Li, *Nanoscale*, 2012, **4**, 1463–1466.
110 K. Shin, J. B. Yoob and J. H. Park, *J. Power Sources*, 2013, **225**, 263–268.
111 H. Zhu, B. Yang, J. Xu, Z. Fu, M. Wen, T. Guo, S. Fu, J. Zuo and S. Zhang, *Appl. Catal., B*, 2009, **90**, 463–469.
112 T. K. Sung, J. H. Kang, D. M. Jang, Y. Myung, G. B. Jung, H. S. Kim, C. S. Jung, Y. J. Cho, J. Park and C. L. Lee, *J. Mater. Chem.*, 2011, **21**, 4553–4561.
113 J. Liao, S. Lin, N. Pan, D. Li, S. Li and J. Li, *Chem. Eng. J.*, 2012, **211–212**, 343–352.
114 X. Zhang, K. Huo, L. Hu, Z. Wu and P. K. Chuw, *J. Am. Ceram. Soc.*, 2010, **93**, 2771–2778.
115 Q. Li and J. K. Shang, *Environ. Sci. Technol.*, 2010, **44**, 3493–3499.
116 L. Yang, S. Luo, R. Liu, Q. Cai, Y. Xiao, S. Liu, F. Su and L. Wen, *J. Phys. Chem. C*, 2010, **114**, 4783–4789.
117 Q. Huang, F. Kang, H. Liu, Q. Lia and X. Xiao, *J. Mater. Chem. A*, 2013, **1**, 2418–2425.
118 M. a. Quintana, T. Edvinsson, A. Hagfeldt, G. Boschloo and T. Edvinsson, *J. Phys. Chem. C*, 2007, **111**, 1035–1041.
119 C. H. Hsu, C. H. Chen and D. H. Chen, *J. Alloys Compd.*, 2013, **554**, 45–50.
120 H. Kim, M. Seol, J. Lee and K. Yong, *J. Phys. Chem. C*, 2011, **115**, 25429–25436.
121 C. W. Zou, Y. F. Ra, A. Alyamani, W. Chu, M. J. Chen, D. A. Patterson, E. A. C. Emanuelsson and W. Gao, *Langmuir*, 2010, **26**, 11615–11620.
122 M. Seol, H. Kim, W. Kim and K. Yong, *Electrochem. Commun.*, 2010, **12**, 1416–1418.
123 K. Sivula, F. L. Formal and M. Grtzel, *ChemSusChem*, 2011, **4**, 432–449.
124 W. Wu, S. Zhang, X. Xiao, J. Zhou, F. Ren, L. Sun and C. Jiang, *ACS Appl. Mater. Interfaces*, 2012, **4**, 3602–3609.
125 H. Yu, X. Li, X. Quan, S. Chen and Y. Zhang, *Environ. Sci. Technol.*, 2009, **43**, 7849–7855.
126 J. Shi, Y. Hara, C. Sun, M. A. Anderson and X. Wang, *Nano Lett.*, 2011, **11**, 3413–3419.
127 M. Shi, X. Pan, W. Qiu, D. Zheng, M. Xu and H. Chen, *Int. J. Hydrogen Energy*, 2011, **36**, 15153–15159.
128 Y. H. Chen, W. S. Li, C. Y. Liu, C. Y. Wang, Y. C. Chang and L. J. Chen, *J. Mater. Chem. C*, 2013, **1**, 1345–1351.